

Cambrian mafic and granitic intrusion in the Ma'ar-Tian hinterland, Weikang Orogenic Belt: Constraints on the tectonic evolution of the Pro-Tethyan Ocean



Xiao-Qiang Li^a, Chan-Lin Zhang^{a,*}, Xian-Tao Ye^a, Haibo Zou^{b,c}, Xiao-Shan Hao^a

^a College of Oceanography, Hohai University, Nanjing, 210098, China

^b Department of Geosciences, Auburn University, Auburn, AL, 36849, USA

^c State Key Laboratory of Continental Dynamics, Department of Geology, Northwest University, Xi'an, 710069, China

ARTICLE INFO

Article history:

Received 13 July 2019

Received in revised form

8 September 2019

Accepted 19 September 2019

Available online 9 October 2019

Keywords:

Cambrian dolerite/gabbro and granite

Age

Geochemistry

Weikang Orogen

Pro-Tethyan Ocean

ABSTRACT

The Weikang Orogenic Belt (WKO) carries information about the evolution of the Pro-Tethyan Ocean. In order to have a better understanding of the early Paleozoic tectonic evolution of the WKO and to unravel the process of the Tarim and Gondwana tectonic field evolution, petrography, age, chemical and Sr-Nd-Hf isotopic composition of the newly identified Cambrian mafic and granitic intrusion in the Ma'ar-Tian hinterland (MZT-TSHT) are investigated. The intrusion of the WKO. O-rincon U-Pb dating reveals that the mafic and granitic rock in Tian hinterland (TSHT) emplaced at ca. 530 Ma, and that the mafic rock in the Ma'ar-Terrane (MZT) emplaced at ca. 500–490 Ma. Whole-rock major and trace element geochemistry defines a holeii igneous rock. In particular, the TSHT mafic rock has depleted Nd isotopic composition with initial ϵ_{Nd} values ranging from 2.74 to 3.60, whereas the MZT mafic rock exhibits enriched whole-rock Nd isotopic composition with ϵ_{Nd} values ranging from -12.90 to -9.71. The distinct chemical and isotopic signatures have the Cambrian mafic rock in the TSHT derived from a depleted mantle source in an initial tectonic setting, whereas the mafic rock from MZT derived from an enriched b-concentrated lithospheric mantle source in an arc setting. The Cambrian granite in the TSHT has typical fractionated light rare earth elements signature, in line with their Nd-Sr-Hf isotopic composition. The Cambrian granite are most likely generated by partial melting of Mesoproterozoic (0.9–1.3 Ga) crustal source and underplating of the coeval mafic magma. Overall in combination with previous studies, the Cambrian mafic and granitic rock in the MZT-TSHT are generated by the high-temperature tectonic evolution of the Pro-Tethyan Ocean initiated at ca. 530 Ma. The long-term high-temperature tectonic evolution led to the formation of the major early Paleozoic accretionary belt in WKO. The Pro-Tethyan Ocean finally closed at ca. 440 Ma as demonstrated by the amphibolite facies metamorphism of the accretionary complex and the middle-late Devonian molasse unconformable overlying the accretionary complex. This process caused the block in East Asia, including the Tarim, Qaidam and North Qilian, Yangtze and Indochina, to dock at the northern fringe of the East Gondwana.

© 2019 Elsevier B.V. All rights reserved.

1. Introduction

The micro-continents distributed in East Asia, including the Tarim, Qaidam, Qilian, South China, North China and Indochina, were believed to have been amalgamated to East Gondwana in the early Paleozoic due to the closure of the Pro-Tethyan Ocean distributed along the Weikang Orogen, Altai, North Qilian, North

Qinling and the Cathaysia (Pan and Wang, 1994; Ma et al., 1996; Pan, 1996; Ma and Schneider, 2000; Xiao et al., 2002a, 2005; Zhang et al., 2004; Li et al., 2018; Zhao et al., 2018). One of the major tectonic units of the Tibetan Plateau and the central orogenic belt in China (i.e., the Weikang Orogen-Ea-Kang Orogen-Qinling-Dabie-Silurogen, see Jiang et al., 1992), the Weikang Orogenic Belt (WKO) plays a key role for understanding of the evolution of the Pro-Tethyan Paleozoic Ocean. Although many studies have been carried out on this orogenic belt, many issues regarding its early Paleozoic tectonic evolution remain unclear, such as the tectonic evolution, the tectonic features of the Precambrian

* Corresponding author.

E-mail address: hangchuanlin@hhu.edu.cn (C.-L. Zhang).

errane and the closing process of the Proterozoic Ocean, and whether or not the Tarim block was emplaced onto the Eastern Gondwana (e.g., Ducea et al., 2003; Jiang et al., 2002, 2008, 2013; Ma et al., 1996; Maern and Schneider, 2000; Pan, 1990; Pan and Wang, 1994; Wang et al., 2001, 2002; Wang, 2004; Xiao et al., 1998, 2002a, b, 2005; Yang et al., 1996; Yin and Harrison, 2000; Yan et al., 2002, 2004, 2005; Zhang et al., 2006, 2007). Especially the bidirectional polarity of the Proterozoic Ocean is under debate. Some geologists favored the northward bidirectional (Wang, 2004; Xiao et al., 2000), and the Paleozoic Kadi-Qiman and Ophiolite are considered as the remnant of the back-arc basin of the Proterozoic Ocean (Wang et al., 2002; Wang, 2004). Another school of ideas suggested the southward bidirectional polarity of the Proterozoic Ocean beneath the South Korean Terrane (SKT), which led to the amalgamation between the North Korean Terrane (NKT) and SKT in the early Paleozoic (Jiang et al., 2002; Maern and Schneider, 2000; Zhang et al., 2018a, b, c, d; Li et al., 2018). In addition, the above north or south bidirectional orientation, some workers proposed a double-sided bidirectional of the Proterozoic Ocean model (Xiao et al., 2002a).

The model advocated in the bidirectional polarity of Proterozoic Ocean were invoked on the following prerequisites: (1) the SKT as a Precambrian microcontinent, therefore the arc-related granite can be formed and (2) the Paleozoic magmatic rock in the WKOB extend to be younger than northward and (3) the magmatic rock in the Tianhishai Terrane (TSHT) are all emplaced during Mesozoic and no Paleozoic magmatism occurred. Moreover, considering the Kangdian Fals, the boundary between the SKT and TSHT, they were separated from the closure of a branch of the Paleozoic Ocean (Ducea et al., 2003; Jiang et al., 2013; Reel et al., 2017), while others claimed that they either a northward or a southward accretion (Xiao et al., 2002a, b, 2005; Wang, 2004). However, our recent work reveals that the main part of the SKT, i.e., the Saijia Group, as a Paleozoic accretionary complex which was separated from the southward bidirectional of the Proterozoic Ocean (Zhang et al., 2018c), and the only confirmed Precambrian basement in the WKOB were the Archean Maar Terrane (MZT, Fig. 1a, Zhang et al., 2018a) and the Neoproterozoic TSHT (Fig. 1a, Zhang et al., 2018c). More importantly, the Early Paleozoic igneous rock, including dolerite, gabbro and granite were identified in the confirmed Precambrian basement, i.e., the Maar Terrane-Tianhishai Terrane (MZT-TSHT). The newly identified Early Cambrian magmatic rock in the MZT-TSHT provide a more reliable reconstruction of the Paleozoic tectono-magmatic evolution history of the WKOB. In this contribution, we report field observations, age, and geochemistry of the newly identified Early Paleozoic dolerite/gabbro and granite in relation to the Archean MZT and central part of the TSHT, in order to constrain the tectonic igneous evolution of the NE Pamir and WKOB and better understand the tectonic evolution of the Proterozoic Ocean and an emplaced process between the Tarim and Eastern Gondwana.

2. Regional geology and petrography

The WKOB, adjoin the Tarim Basin to the north, the Tibetan Plateau to the east, and the Pamir Plateau to the west, is off-set from the East Korean Orogen and Songpan-Gan-Terrane by the Alpinic tectonic collision of the east (Fig. 1a, Gibbon et al., 2015; Yin and Harrison, 2000). Tectonically, the WKOB can be divided into the eastern and western sections. The western section, generally known as the Pamir alien, has been divided into three tectonic units, i.e., the North Pamir, Central Pamir, and South Pamir (Robin et al., 2007, 2012; Schabert et al., 2004). The 1/250,000 mapping and other tectonic geochronological data in this area demonstrate that the main part of the NE Pamir (i.e., Ta hikorgan

Terrane (TSKT) shown in Fig. 1a) is composed of a Cambrian volcanic-arc magmatic sequence, locally known as the Binkole Group (BKG), rather than a Triassic accretionary complex (e.g., Robin et al., 2012). At the northern margin, the BKG is on the newly identified Archean MZT (Fig. 1a, Ji et al., 2011; Zhang et al., 2018b).

The eastern section of the WKOB can be divided into three main tectonic units (Fig. 1a), i.e., the NKT, the SKT and the TSHT, by the Paleozoic Kadi-Qiman and Ophiolite (KQS), Maar-Kangdian Fals (MKF) and Honghanh-Qiaoerlanhan Series (HQS), respectively (Maern and Schneider, 2000; Xiao et al., 2005). The NKT, an uplifted errane of Tarim Block, composed of a pre-Nanhuanian metamorphosed and deformed basement and unconformably covered by Nanhua-Cambrian carbonate-clastic sequence (Zhang et al., 2007, 2016). The main part of SKT, i.e., the Saijia Group, as a metamorphosed Cambrian or early Ordovician accretionary wedge and remnant of the BKG in rock an emplaced, age, metamorphic grade and deformation feature (Fig. 1a, Zhang et al., 2018c, d). Thus, the BKG and the Saijia Group composed a major early Paleozoic accretionary wedge identified between the Tarim and the MZT-TSHT (Fig. 1a). The TSHT is identified by glacier deposits and knowledge of its geological high incompleteness of geographic remnant (Cie et al., 2006). Some scholars suggested that the errane is related to the Songpan-Gan block of Tibetan Plateau, which collided with SKT during the Early Mesozoic (Xiao et al., 2005; Li et al., 2015). The Neoproterozoic Tianhishai Group (Ongederialirong peak at ~743 Ma, Zhang et al., 2018c), as the only Precambrian sequence of the TSHT, composed of meta-gneiss and limestone and is in fact unconformably connected with the late Paleozoic or early Mesozoic accretionary wedge (Zhang et al., 2018c). The thick monotonous and parallel metamorphosed sequence of clastic marine deposits host the igneous (Maern and Schneider, 2000).

The Early Paleozoic and Mesozoic magmatic rock associated with the evolution of the Proterozoic and Paleozoic Ocean are widespread in the WKOB. Previous studies focused on the igneous rock and some key geological units such as the ophiolite along the Xinjiang-Tibet road and the China-Pakistan road of the difficult accessibility area of the WKOB (e.g., Maern and Schneider, 2000; Wang et al., 2002, 2017; Yang et al., 1996; Zhang et al., 2004, 2005, 2016; Li et al., 2015; Jiang et al., 2013). The detailed research on the Early Paleozoic magmatic rock in the WKOB are identified mainly in the SKT and subordinate in the NKT, while the Mesozoic magmatic rock in the WKOB are emplaced mainly along the northern part of the SKT and the northern margin of the TSHT (Fig. 1a). The Early Paleozoic graniteoids were emplaced in the SKT during 510–400 Ma (Jiang et al., 2002, 2008; Zhang et al., 2018a, 2018b). Geochemically, the early Paleozoic granite in SKT can be defined as a dioritic and peralitic, i.e., the 510–450 Ma low-potassium granite and the 430–400 Ma high Ba–Sr and Al-potassium granite (Ye et al., 2008; Yan et al., 2002, 2005). In combination of the ca.440 Ma amphibolite-facies metamorphism of the SKT, the accretion between Tarim and SKT were finished at ca.440 Ma (Zhang et al., 2018c).

The MZT is located at the northern margin of the NE Pamir (Fig. 1a), where the Archean basement in the WKOB is identified (Ji et al., 2011; Zhang et al., 2018b). The Neoproterozoic sequence is intruded by the peralitic granite, including the Neoproterozoic rhyolite and granodiorite and Cambrian dolerite-gabbro and Mesozoic granite (Fig. 1b, Zhang et al., 2018b; his study). To the north of the errane is the Cambrian accretionary wedge (i.e., the BKG, Zhang et al., 2018a) and a northern margin, identified by the Mesozoic granite. The dolerite-gabbro are mostly identified as the northern margin of the MZT, host a rock and dike in the field. The rock outcrop is a form

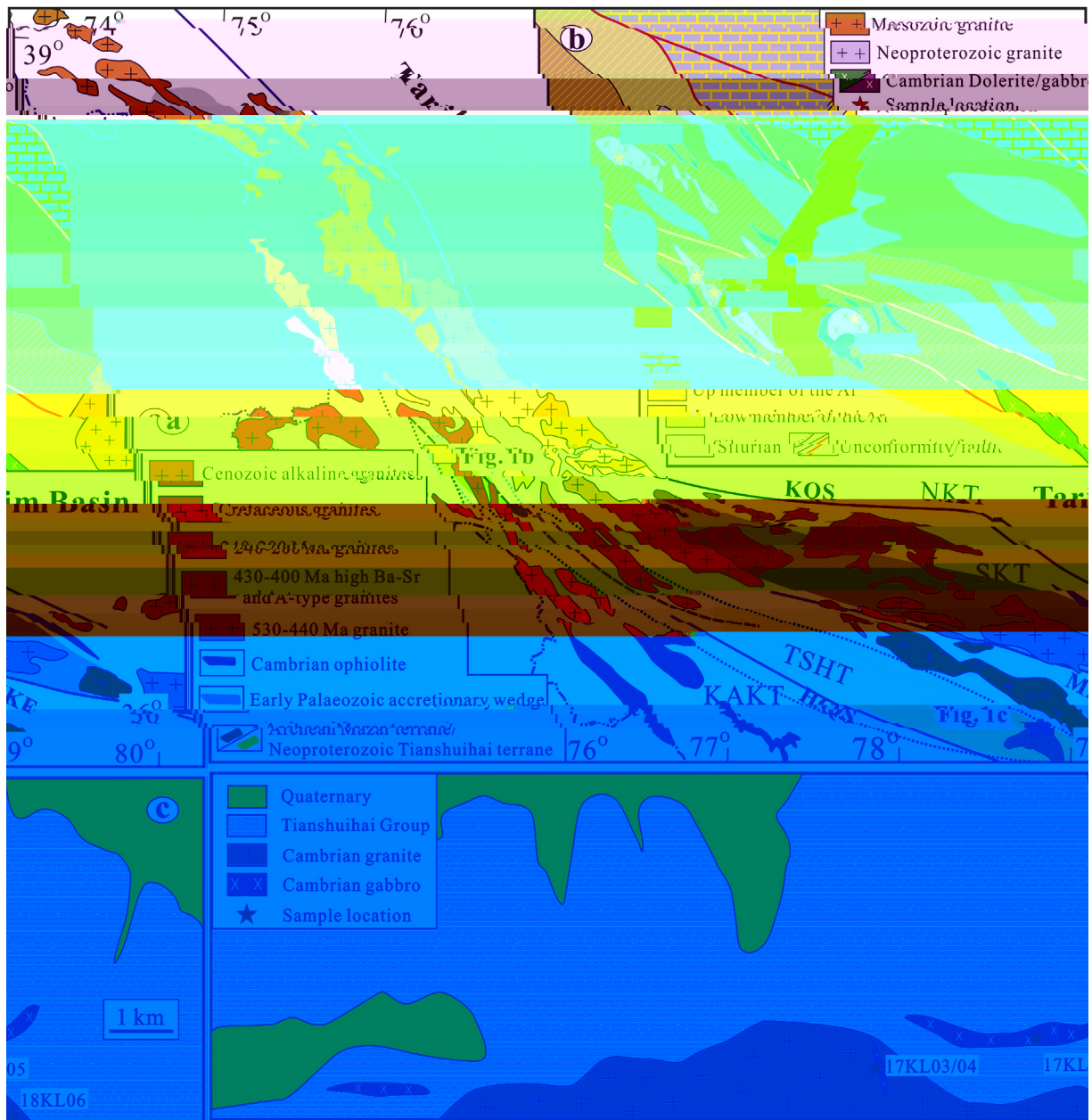


Fig. 1. (a) Simplified tectonic map of the Weibei Orogenic Belt (WOB), showing the major terrane and related granite types (Modified from Zhang et al., 2018d). The so-called basement of TSKT and SKT, locally known as the Binkole Group and Sailla Group, are an early Paleozoic accretionary wedge. NKT—Northern Kailash terrane; SKT—Southern Kailash terrane; TSKT—Tianhishai terrane; TSHT—Tianshuihai terrane; MZT—Ma'ar Terrane; KQS—Kadi-Qiman Terrane; MKF—Ma'ar-Kanglifa Terrane; HQS—Honghanh-Qiaojianhan Terrane. (b) Geological map of the Cambrian mafic rocks in the Ma'ar terrane. (c) Geological map of the Cambrian magmatic rocks in the Tianshuihai terrane.

in the general area are kilometers. The dike morphology in NW and are several hundred meters or more than 1 km long and several hundred meters wide (Fig. 1b).

The TSHT is a NW-SE trending belt, located on the north of Kanglifa (Fig. 1a). Magmatic rocks in the TSHT were emplaced mainly during Triassic-Jurassic (240–195 Ma) and subordinate during the Early Cambrian (Fig. 1a, He et al., 2016 and his study). The Early Cambrian dolerite-gabbro in this region are distributed on the Dahongliang iron deposit district, central part of the TSHT (Fig. 1c, He et al., 2016). The dolerite-gabbro occur as dikes in the field, strike in EW and are several hundred meters or several kilometers long and several dozens of meters wide (Fig. 1c). Zircon LA-ICPMS dating of a gabbro sample near the sample location of this region yielded age of 532.3 ± 3.1 Ma

(He et al., 2016).

The dolerite/gabbro and granite were collected at the MZT (Fig. 1b) and central part of TSHT (Fig. 1c). The dolerite/gabbro samples were analyzed to a certain degree identified in the thin section and the electron probe analysis (see details in section 4.2), which a replacement of clinopyroxene by hornblende and enrichment of the plagioclase. The gabbro samples consist of pyroxene (all replaced by the hornblende), having a pyroxene polymorph and plagioclase (Fig. 2a), and consist mainly of hornblende (40–60%), enriched plagioclase (40–50%) and minor Ti-Fe oxide. The dolerite are composed mainly of hornblende (50–65%), enriched plagioclase (30–50%). The granite are relatively fresh high enriched enrichment of the plagioclase (Fig. 2b). They are composed mainly of K-feldspar (50–55%), plagioclase

(10–15%), quartz (30–35%) and minor secondary minerals, including accessory minerals of zircon and apatite.

3. Analytical procedures

Zircon separation was carried out using standard crushing, sieving, and heavy liquid and magnetic separation techniques. Representative zircon concentrates were obtained on a double-ended amphibole hand-picking under a binocular microscope. Zircon dating of three samples was carried out at Tianjin Institute of Geology and Mineral Resources (TJIGMR), Chinese Geological Survey (CGS), where a Neptune MC-ICPMS equipped with a 193 nm excimer laser ablation system was used to determine zircon U–Pb ages. The detailed analytical procedures are similar to those of [Geng et al. \(2011\)](#). Zircon dating of a gabbro sample from MZT was conducted on a SHRIMP-II instrument at Beijing SHRIMP Centre (National Science and Technology Infrastructure), using the standard operating condition ([Williams, 1998](#)). Ion plots ([Ludwig, 2003](#)) are used for data processing. Zircon U–Pb isotope data are listed in [Table S1 and S2](#).

Mineral compositions were determined on thin sections using an automated JEOL 8800 electron microprobe equipped with 5 wavelength spectrometers at Guangzhou Institute of Geochemistry, Chinese Academy of Science. The operating conditions during analyses are 15 keV accelerating voltage and 15 nA beam current with 20 counting time. The analytical precision is better than 5%. The analytical results of hornblende are listed in [Table S3](#).

Major elements were obtained using Rigaku ZSX100e X-ray fluorescence (XRF) on fused glass beads at the Nanjing Institute of Geology and Mineral Resources (NJIGMR), CGS, following analytical procedures similar to those of [Liu et al. \(2006\)](#). Analytical precision is better than 5%. Trace elements were analyzed using a PE Elan 600 ICP-MS at the Institute of Geochemistry, Chinese Academy of Science, following procedures similar to those described by [Liu et al. \(2006\)](#).

18KL06 field variable U (720–3065 ppm) and Pb (66–283 ppm) content and high relative $^{232}\text{Th}/^{238}\text{U}$ ratio (0.27–1.80, Table S2), similar to typical magmatic iron. All the 29 analyses yield concordant $^{206}\text{Pb}/^{238}\text{U}$ age and $^{207}\text{Pb}/^{235}\text{U}$ age and form a high cluster on the concordia diagram with a weighted mean $^{206}\text{Pb}/^{238}\text{U}$ age of 532.7 ± 2.5 Ma (Fig. 3d, MSWD = 0.24).

4.2. Mineral geochemistry

A total of 33 analyses were carried on the hornblende from MZT gabbroic diorite (2016KL17B and 15D071H5). The relative high Si (7.33–7.93) and Ca (1.77–2.03) apf (atoms per formula unit) and belong to calcic amphibole according to the classification scheme of Leake et al. (1997). The $(\text{Na} + \text{K})_{\text{A}}$ (occupancy of Na + K in A-site, less than 0.5), and are mainly actinolite and magnesiohornblende (Fig. 4a). Their $(\text{Na} + \text{K})_{\text{A}}$ and $^{\text{IV}}\text{Al}$ (occupancy of Al in tetrahedral site) hardly decrease with decreasing TiO_2 (Fig. 4b, c), similar to the concordant trend of amphibole from the Iberian appinite (Molina et al., 2009).

4.3. Whole-rock elemental geochemistry

The MZT dolerite/gabbroic sample has a large range of SiO_2 (47.88–55.36%), Al_2O_3 (11.48–15.58%), CaO (6.02–14.74%), MgO (2.73–10.78%) and $\text{Fe}_2\text{O}_3^{\text{T}}$ (9.88–13.39%). Their Na_2O (0.74–5.16%) contents are generally higher than K_2O (0.21–1.30%). Deo is a variable hydrothermal alteration, especially the immobile incompatible elements of the rock type and to decipher their geochemical signature. On the Nb/Y versus Zr/ TiO_2 plot (Fig. 5a), all the samples plot within the basaltic field. On the AFM diagram, they define a typical holeii trend (Fig. 5b). Their $\text{Mg}^{\#}$ range from 35 to 65 degrees of crystallization and/or crystallization conditions (see following discussion). On the Harker diagram

(Fig. 6), SiO_2 , TiO_2 , P_2O_5 , total REE increase while Cr and Ni decrease with decreasing $\text{Mg}^{\#}$, whereas Al_2O_3 , $\text{Fe}_2\text{O}_3^{\text{T}}$, Na_2O , CaO and Zr are not correlated with $\text{Mg}^{\#}$. On the chondrite-normalized REE plot, the diorite-enriched LREE pattern is similar to that of an (La/Yb)_N (2.67–6.87) ratio (Fig. 7a). Most MZT mafic samples lack significant E anomalies ($E/E^* = 0.81\text{--}1.17$). Normalized to primitive mantle, all samples show arc-like patterns with variable enrichment in incompatible trace elements and significant Nb–Ta trough (Nb/La = 0.30–0.44) and variable negative P anomalies (Fig. 7b).

The TSHT mafic intrusion exhibits relative uniform SiO_2 (46.82–49.68%) and varying Al_2O_3 (14.67–18.16%), CaO (5.47–11.20%), MgO (5.84–10.20%) and $\text{Fe}_2\text{O}_3^{\text{T}}$ (8.20–11.69%). They are sodium-rich (2.12–4.29% Na_2O) relative to K_2O (0.23–2.99%). The TSHT mafic rock has variable Ni (12–156 ppm) and Cr (7–448 ppm) contents (Supplementar Table 3). All samples plot within the basaltic field on the Nb/Y versus Zr/ TiO_2 plot (Fig. 5a). On the AFM diagram (Fig. 5b), they define a typical holeii signature. On the Harker diagram (Fig. 6), the Na_2O , TiO_2 , P_2O_5 , Zr and total REE increase while Cr, Ni and CaO decrease with decreasing $\text{Mg}^{\#}$ and SiO_2 , Al_2O_3 remain constant. The TSHT mafic intrusion has variable total REE abundance (70.68–225.08 ppm). The diorite-enriched LREE pattern is similar to that of an (La/Yb)_N ratio ranging from 4.71 to 17.4 on the chondrite-normalized REE diagram (Fig. 7c). Most TSHT mafic samples show slight negative europium anomalies ($E/E^* = 0.95\text{--}1.29$). All samples

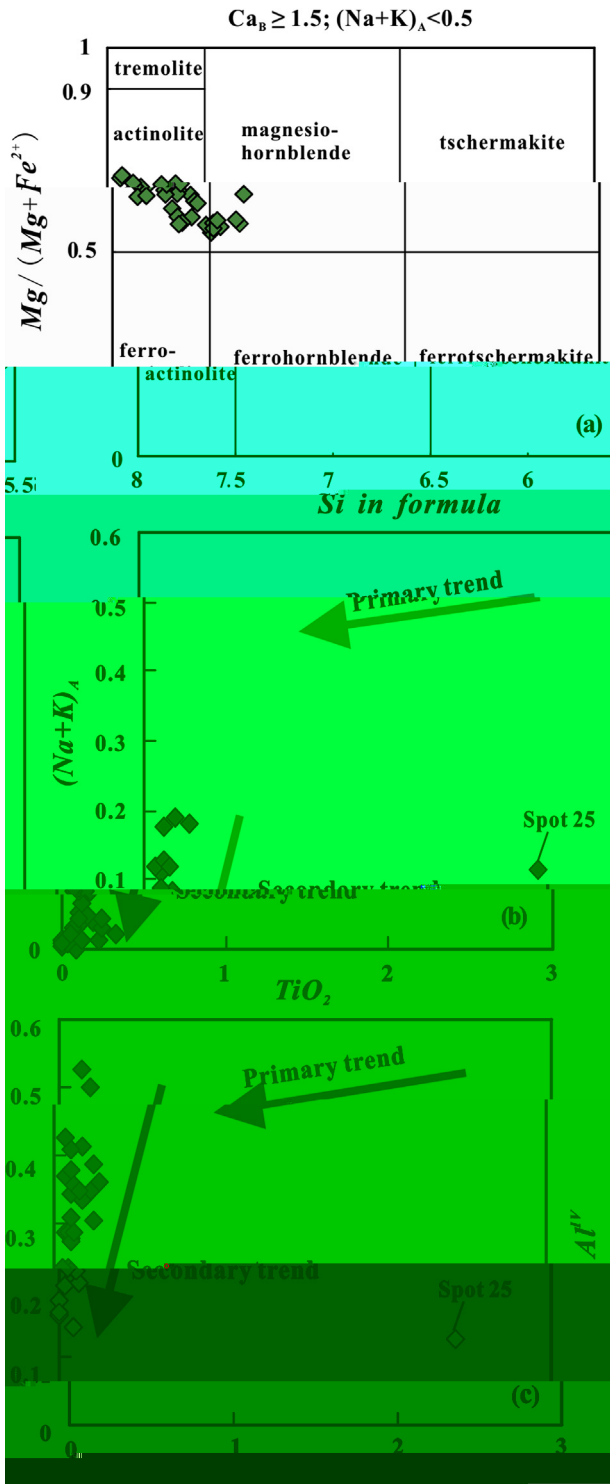


Fig. 4. (a) Classification of hornblende (Leake et al., 1997); (b) TiO_2 (%) vs. Al^{IV} and (c) TiO_2 (%) vs. $(Na+K)_A$ diagram of the hornblende showing the secondary trend.

On the TAS diagram (Fig. 5c), the plot is in the field of granite. The sample contains Al_2O_3 (11.80–13.85%), TiO_2 (0.05–0.15%), MnO_2 (0.01–0.03%), MgO (0.06–0.52%) and P_2O_5 (0.01–0.02%). Major elements define their peraluminous igneous rocks with A/NK ranging from 1.10 to 1.24 and A/CNK ranging from 1.04 to 1.13. The TSHT granite has a total REE abundance ranging from 120 to 241 ppm. The exhibits a relatively flat REE pattern on the

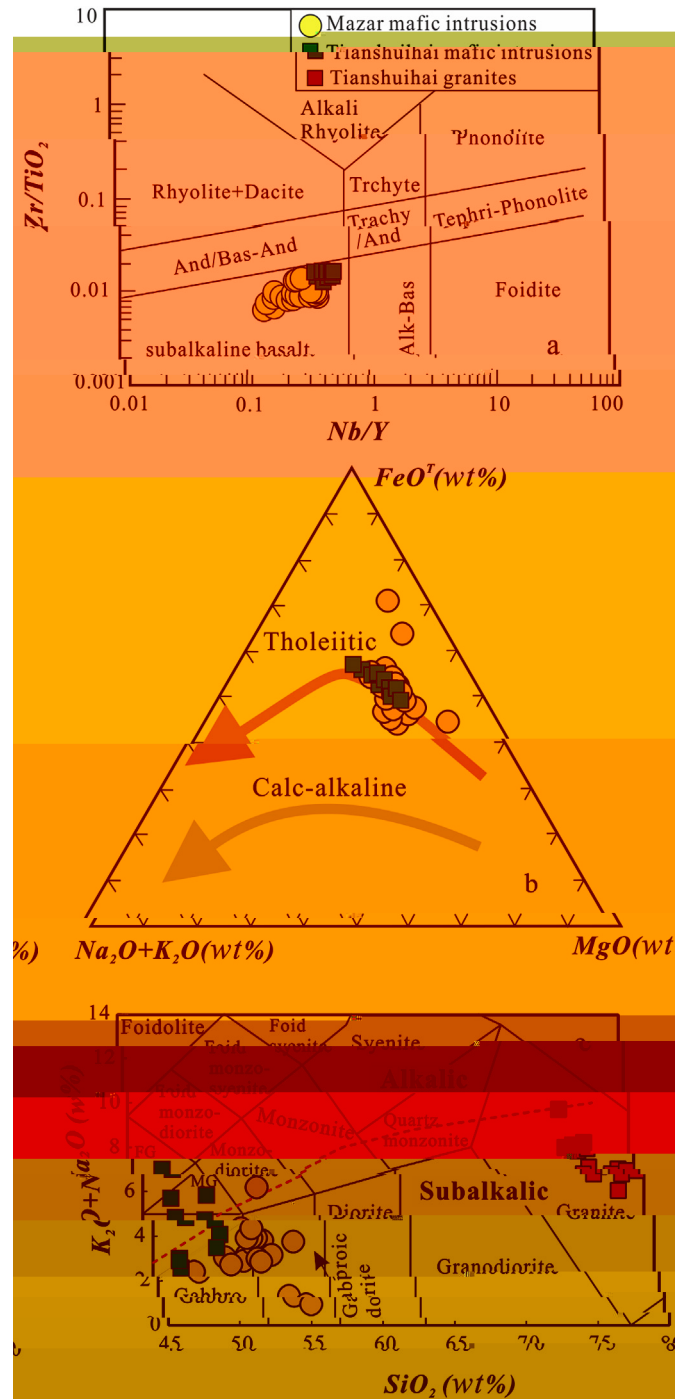


Fig. 5. (a) Nb/Y vs. Zr/TiO₂ classification, (b) AFM and (c) TAS diagram of the dolerite-gabbro and granite from Mazar Terrane-Tianshuihai Terrane.

chondrite-normalized REE diagram (Fig. 7e), which $(La/Yb)_N$ ratio ranging from 2.61 to 7.19 and high negative E anomalies ($E/E^* = 0.02-0.09$), likelihood of plagioclase fractionation. Normal and primitive mantle, all samples show enrichment in large ion lithophile elements such as Rb, Th, La and depletion in Ba, Sr, P, Ti and E (Fig. 7f).

4.4. Zircon in situ Lu–Hf isotopic compositions

A total of 57 in situ Lu–Hf isotopic analyses were carried on the dated zircon from TSHT granitic samples (17KL04 and 18KL06,

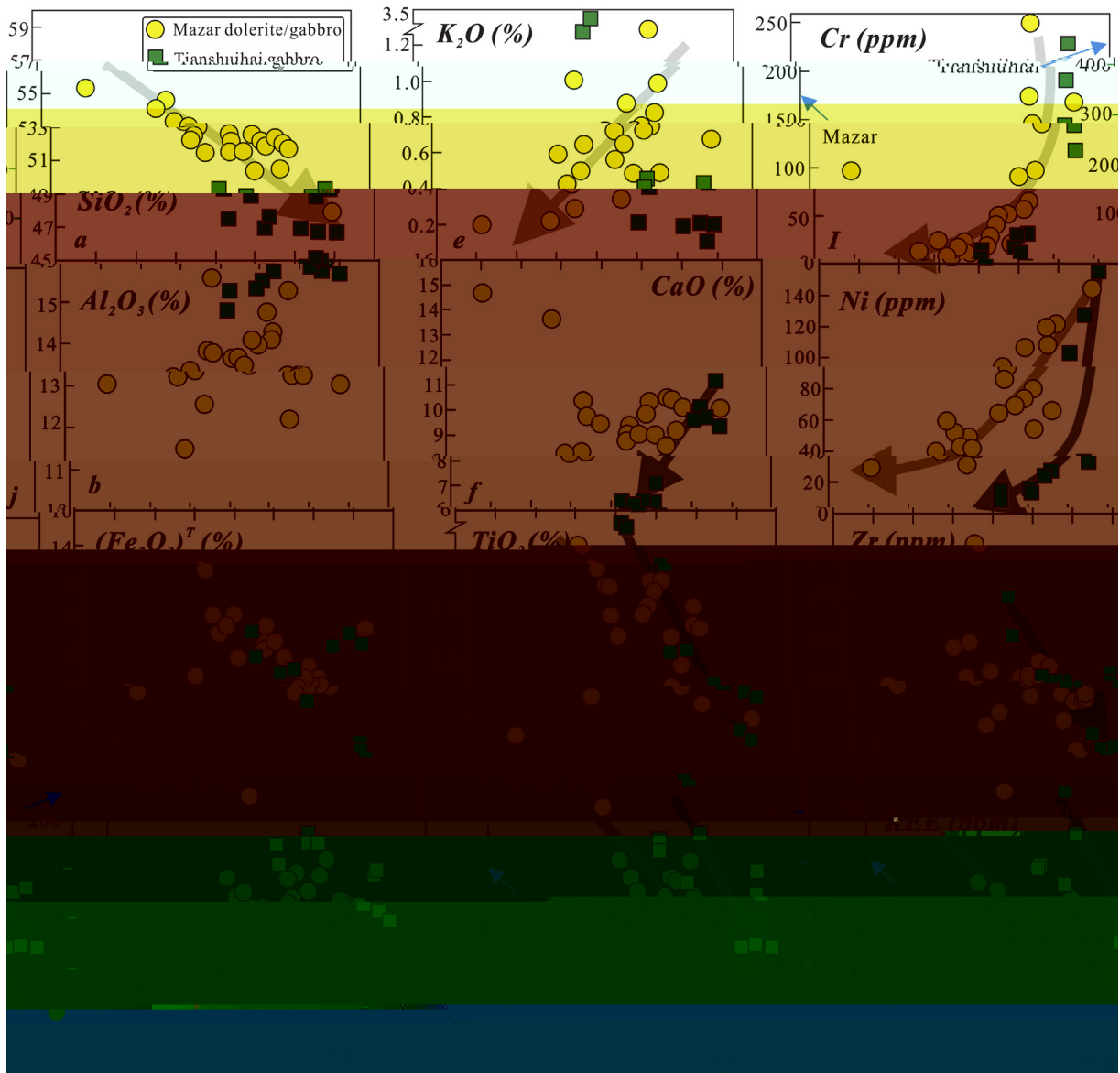


Fig. 6. Harker diagram for the Cambrian mafic intrusive rock from Mazar-Tianshuihai terrane.

Table S5). All analyses show positive initial $\epsilon_{\text{Hf}}(t)$ values ranging from 2.6 to 9.2 (most between 4 and 8) and exhibit a general Gaussian distribution (peak at 5, Fig. 8a) and Mesoproterozoic or older model age ($T_{\text{DM}2}$) ranging from 905 to 1324 Ma (Fig. 8b).

4.5. Sr–Nd isotopic compositions

The MZT dolerite/gabbro sample has negative $\epsilon_{\text{Nd}}(t)$ values (-12.90 to -9.71) and variable initial $^{87}\text{Sr}/^{86}\text{Sr}$ values (0.7107–0.71517, Table S6, Fig. 9a). The TSHT mafic rock has positive $\epsilon_{\text{Nd}}(t)$ values ranging from 2.74 to 3.60, and their initial $^{87}\text{Sr}/^{86}\text{Sr}$ values ranging from 0.70597 to 0.70847. As for the Cambrian TSHT granite, they exhibit $\epsilon_{\text{Nd}}(t)$ values ranging from -0.39 to 1.08, and initial $^{87}\text{Sr}/^{86}\text{Sr}$ values ranging from 0.7039 to 0.71229. We notice the significant decoupling between the whole-rock Nd and Sr isotope composition for the MZT mafic rock, which could be attributed to emplacement hydrothermal alteration (e.g., McCulloch et al., 1981) a demonstrated by their enrichment in amphibole and hornblende chemical composition. Thus, the Sr isotope of the MZT mafic rock are not suitable for

reconstruction on the petrogenesis of the mafic rock. On the $\epsilon_{\text{Nd}}(t)$ vs. $\epsilon_{\text{Hf}}(t)$ diagram (Fig. 9b), the TSHT granite shows broad coupled whole-rock Nd and Hf isotope.

5. Discussions

5.1. Petrogenesis of the mafic rocks

5.1.1. Hydrothermal alteration

As indicated by their high LOI (most higher than 2%), secondary mineral observed in their section and apparent secondary trend for the amphibole (Fig. 4b, c), the MZT-TSHT mafic rock underwent a variable degree of alteration after emplacement, which may have changed the concentration of some incompatible elements and their enhanced mobility. Since Zr is considered to be immobile during low-grade hydrothermal alteration and metamorphism of igneous rock, it has been used as a reference for dating the mobility of other trace elements (Pearce et al., 1992). We investigated the correlation between Zr and other elements (figure not presented). The result indicates that TiO_2 , Nb, Th, Hf, Y,

Ta and REE correlate well with Zr, suggesting relative immobility of these elements during post-emplacemen processes. Some LILE, such as Ba, Rb and Sr, however, show no correlation with Zr, indicating their mobility. Thus, the conclusion is that the original magma has not been significantly affected by high field strength elements (HFSE: Th, Nb, Zr, Hf, Ti, Y) and REE. Their variation could be attributed to magmatic processes and can be used for petrogenetic diagnosis.

5.1.2. AFC process

The analysed mafic rock has variable MgO (2.73–10.78% for MZT and 5.84–10.50% for TSHT), Mg[#] (35–65 for MZT and 51–65 for TSHT), Cr (5.88–255 ppm for MZT and 20.0–448 ppm for TSHT), Ni (31.9–145 ppm for MZT and 12.1–156 ppm for TSHT) and total REE abundance (41.5–148 ppm for MZT and 70.7–225 ppm for TSHT), indicating that the crystallized from evolved rather than

primitive magma, probably due to assimilation and fractional crystallization (AFC) processes. As shown in the Harker diagram (Fig. 6), the analysed samples exhibit distinctive correlations between Cr and Mg[#] (Fig. 6i), Ni and Mg[#] (Fig. 6j), indicating fractional crystallization of olivine and/or clinopyroxene. The distinct clinopyroxene-plagioclase control trends in the Pearce elemental ratio diagram (Fig. 10a) confirmed the fractional crystallization of clinopyroxene and plagioclase. The negative correlations between Fe₂O₃ and TiO₂ concentration and Mg[#] are indicative of fractional crystallization of Fe–Ti oxide. AFC processes can produce a positive correlation between ε_{Nd}(t) and Mg[#]. The slight positive correlation between ε_{Nd}(t) and Mg[#] for the MZT mafic rock argues for crystallization before final crystallization. 1

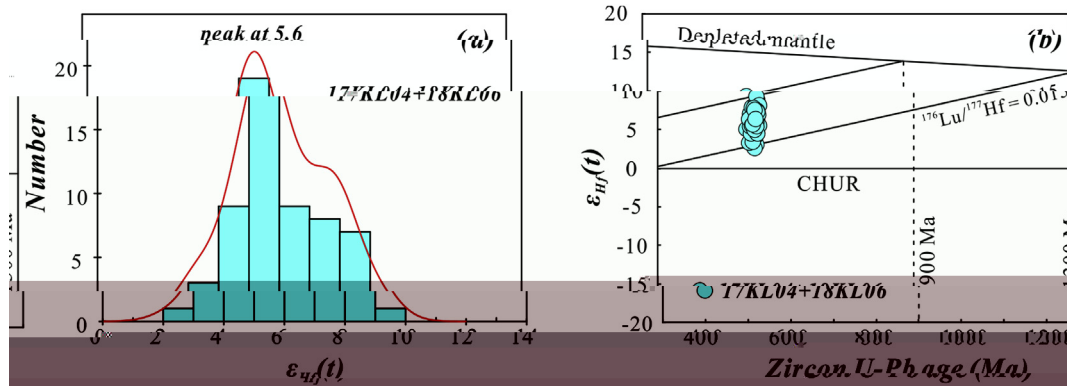


Fig. 8. Zircon $\epsilon_{Hf}(t)$ spectrum (a) and Zircon U–Pb age– $\epsilon_{Hf}(t)$ diagram (b) of the Cambrian granitic intrusion from Tianhishai Terrane.

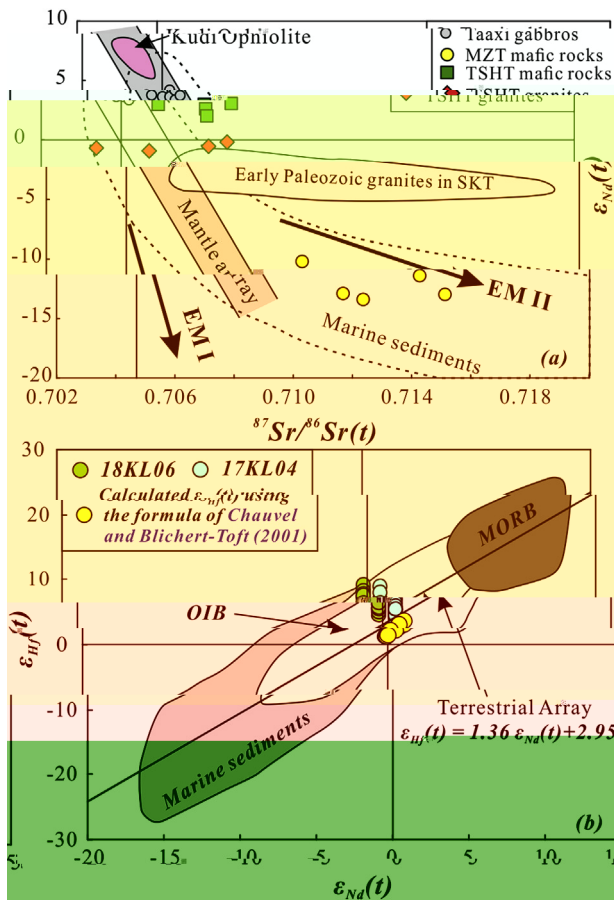


Fig. 9. (a) Whole-rock Sr–Nd isotopic diagram of the Cambrian mafic and granitic intrusion from Ma’ar-Tianhishai Terrane. The Taaxi gabbros are from Zhang et al. (2018d); The So’ukh’nl n Terrane (SKT) granites are from Zh et al., 2017; Liao et al., 2010; Wang et al. (2017), Li et al. (2014); The marine sediments are from Hofmann, 2003; Kidi Ophiolite are from Pan, 1996. (b) Whole-rock $\epsilon_{Nd}(t)$ – $\epsilon_{Hf}(t)$ diagram of the Cambrian granitic intrusion from Tianhishai Terrane, showing the terrestrial array and the field for middle ocean ridge basal (MORB), oceanic island basal (OIB) and global sediments are from Ver o et al., 1999.

been the $\epsilon_{Nd}(t)$ and $Mg^\#$, indicating significant crustal contamination (Fig. 10b). Crustal contamination could imply a negative $\delta^{87}Sr$ and Nb/La ratio which could produce a positive correlation between the $Mg^\#$ and Nb/La. This conclusion is supported by the high positive correlation and no significant correlation between the $Mg^\#$ and Nb/La for the MZT and TSHT mafic

rock, respectively (Fig. 10c). The $(La/Ta)_N$ – $(Th/Ta)_N$ diagram (Fig. 10d) indicates that the contaminated component for the MZT mafic rock is the upper crust.

Therefore, the conclusion has been analyzed mafic sample from TSHT has not undergone significant crustal contamination, whereas the Cambrian rock from MZT has been contaminated by the upper crust component in this region.

5.1.3. Magma sources

The MZT and TSHT are ophiolite Precambrian basements in the WKOB, i.e., the Archean MZT (Zhang et al., 2018b) and the Neoproterozoic TSHT (Zhang et al., 2018c). The different igneous rocks of the Precambrian basements for the MZT and TSHT lead to the conclusion that the ophiolite and different Cambrian mantle sources. The mafic rock from the TSHT has a depleted hole-rock Nd isotopic composition ($\epsilon_{Nd}(t) = 2.74$ to 3.60), and exhibits arc-like hole-rock elemental composition, such as significant Nb–Ta ratio, enrichment of LREE, LILE and depletion of HREE and HFSE (Fig. 7, Rdnick and Gao, 2003). The depletion of the depleted Nd isotopic and the enriched LREE and LILE have more features of the E-MORB and some OIB (e.g., Zhang et al., 2018d). Such features can be attributed to crustal contamination (Rdnick and Gao, 2003), hybridization of magma sources by recycled terrigenous sediment or fluid metasomatism in the bedrock (e.g., Hake or he et al., 1993) or crystallization of Ti-bearing mineral (such as rutile and Ti-bearing amphibole) (e.g., Hange et al., 2010). A mentioned above, crustal contamination can be ruled out. Although fractionation/accumulation of Ti-bearing mineral might have occurred as mentioned above, this is not the key reason to generate the Nb–Ta ratio of the mafic rock from TSHT, because of the positive correlation between the TiO_2 and Nb/La ratio (figure not shown). Thus, the mantle source for the parent magma of the TSHT mafic rock is most likely a contaminated or enriched basaltic or fluid in a bedrock (e.g., Hake or he et al., 1997). Nb/U and Ta/U ratios are commonly used to identify the injection of crustal material in the mantle source or crustal contamination (e.g., Hofmann, 1988). The Nb/U and Ta/U ratios of the TSHT mafic rock are 7.1–23.3 and 0.4–1.3, significantly lower than those of the OIB and MORB (Nb/U > 47 and Ta/U > 2.7, Hofmann, 1988). The low ratios of Nb/U and Ta/U features of the TSHT mafic rock argue for significant injection of crustal material into the depleted mantle source for the TSHT mafic rock, which might be due to bedrock processes. In light of their depleted hole-rock Nd isotopic composition, we propose that they are originated in the initial bedrock during the formation of the Proterozoic Ocean.

Although having undergone upper crust contamination, the MZT mafic rock has a variable $Mg^\#$ number exhibits similar Nb/La

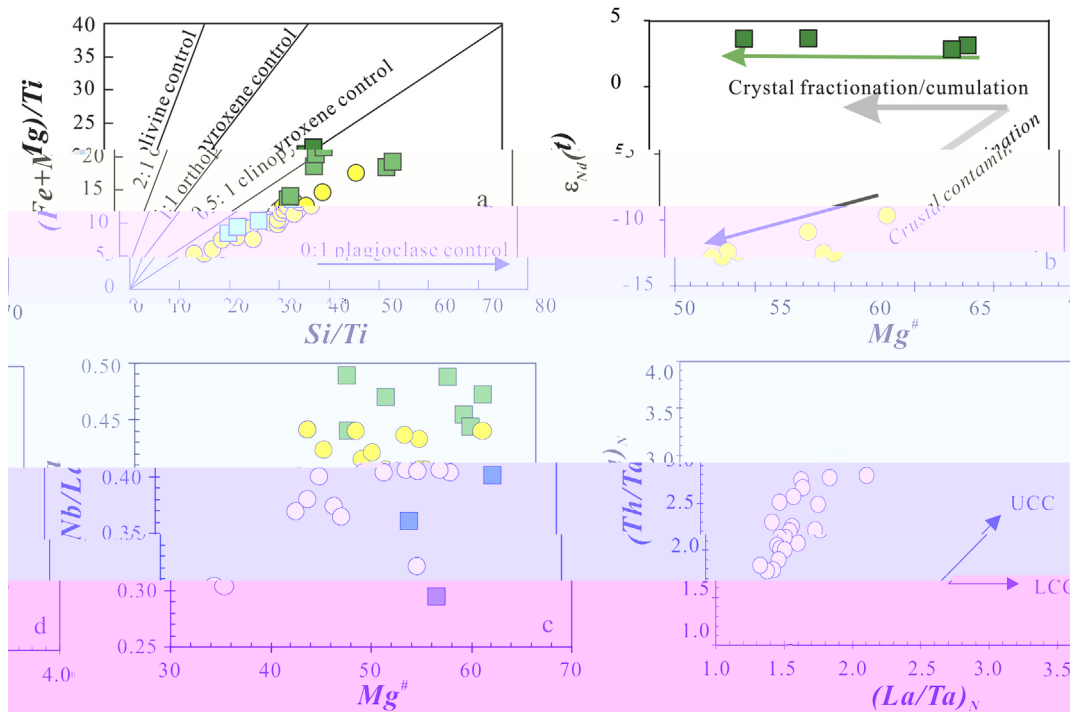


Fig. 10. (a) Si/Ti vs. (Mg + Fe)/Ti (molar ratio) diagram of MZT-TSHT mafic rock showing accumulation of clinopyroxene and plagioclase; (b) Mg[#] vs. ε_{Nd}(t), (c) Mg[#] vs. Nb/La and (d) (La/Ta)_N vs. (Th/Ta)_N diagram illustrating upper continental crust contamination trend for the MZT mafic rock, and no significant contamination for the TSHT mafic rock. UCC – upper continental crust; LCC – lower continental crust.

ratio (0.30–0.46). Thus, their incompatible ratio could broadly reflect their primitive geochemical signature. The REE and incompatible element distribution pattern of MZT mafic intrusion broadly exhibits arc-basaltic signature, characterized by significant Nb–Ta enrichment (Fig. 7), enrichment of LREE, LILE and depletion of HREE and HFSE (Rudnick and Gao, 2003, Fig. 7). Furthermore, their HFSE ratios, such as Th/La and Nb/Th, are also comparable with those of primitive arc-basaltic (Fig. 11, OIB, primitive arc-basaltic and arc magmas from Sun and McDonough, 1989 and Rudnick and Gao, 2003, respectively). Among the MZT mafic rocks, the sample with the negative initial Nd isotopic composition (−9.71)

has high Mg[#] (59), which argues for an isotopically enriched mantle source for the primary magma of the MZT mafic rock. We deduce that the sample derived from an enriched Nb–containing lithospheric mantle (SCLM). As a matter of fact, the Archean MZT pore is a long-term enriched SCLM according to the hole-rock ε_{Nd}(t) value of the Archean mafic volcanic rock (−11.9 to −9.3, recalculated at 490 Ma, Jie et al., 2011), which coincides with the MZT mafic rock. Partial melting of an initially cold SCLM could not occur unless previously modified by the mantle source (Ringwood, 1974). This may be related to the continental (530–490 Ma) or the hard bedrock of the Proterozoic Ocean.

The TSHT mafic rock exhibits positive hole-rock Nd isotopic composition, whereas the MZT mafic rock displays much more enriched hole-rock Nd isotopic composition (ε_{Nd}(t) = −12.90 to −9.71). From the TSHT mafic rock (ca. 530 Ma) of the MZT mafic rock (ca. 490 Ma), the mantle source of the mafic rock may be related to increasing metamorphic degree of the mantle bedrock. This conclusion is further supported by the relatively higher Th/Yb ratio as a given Nb/Yb for the MZT-TSHT mafic rock. All MZT mafic rock plots in the field of continental arc and the TSHT mafic rock plots in the field of continental arc and the mantle-arc on the Nb/Yb vs. Th/Yb diagram (Fig. 12). Comparing with the binary diagram, the triangular diagram could be influenced by crystal fractionation. On the Nb–Zr/4–Y diagram (Fig. 13), the TSHT mafic rock are mostly plotted in the field of high plate hole-like basalts, which is more typical of high plate alkaline basalts, while the MZT mafic rock plots in the field of volcanic arc basalts.

Therefore, the Cambrian TSHT mafic rock were derived from a depleted mantle source in an initial bedrock setting, whereas the Cambrian MZT mafic rock were more likely derived from a bedrock metamorphic SCLM stage in an arc setting.

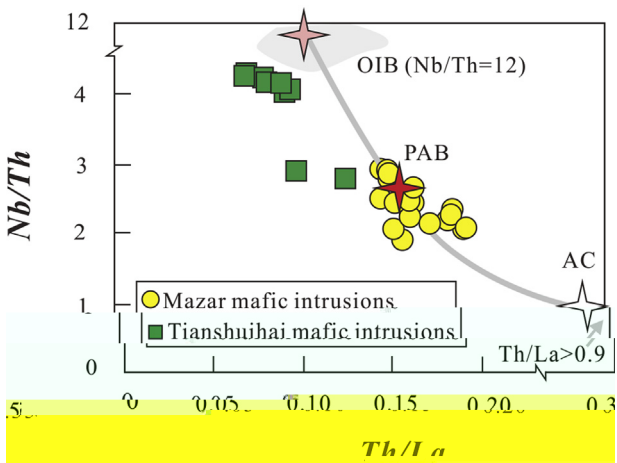


Fig. 11. Th/La vs. Nb/Th diagram. The MZT mafic rock cluster around primitive arc-basaltic (PAB) and the TSHT mafic rock plots in the field of oceanic island basalts (OIB) and PAB. OIB, PAB and arc magmas from Sun and McDonough (1989) and Rudnick and Gao (2003), respectively.

A common accessory mineral in magmatic rock, apatite has different solubility in different magma types (e.g., Li et al., 2007). Apatite has a higher solubility in mafic magma than in felsic magma and crystallizes early during the fractionation of magma, which results in a negative relationship between P and SiO₂. While in the mafic magma, apatite has an opposite behavior and leads to apatite either remaining unchanged as the SiO₂ increases (Wolf and London, 1994). This different behavior of apatite in mafic magma and felsic magma can be used to discriminate I- and S-type granites (Wheeler et al., 2003). The TSHT granites exhibit low concentrations of P₂O₅ (<0.02%, Fig. 14b), indicating low I-type granite affinity. In addition, all TSHT granitic samples plot in the I-type granite field on the Zr vs. TiO₂ diagram (Fig. 14c). Therefore, we conclude that the Cambrian TSHT granites are high-*K* I-type granites.

The negative E anomalies ($E/E^* = 0.02-0.09$) and low concentrations of Sr (21.9–71.5 ppm) suggest fractional crystallization of plagioclase. The apparent negative Ba, Sr, P and Ti anomalies in the primitive-mantle-normalized trace element and REE chondrite-normalized diagram for the TSHT granites (Fig. 7) indicate fractional crystallization of plagioclase, apatite and Fe–Ti oxide during magma evolution. Furthermore, plots of process index diagram on log Ba vs. log Rb (Fig. 14d) yield trends of crystal fractionation of plagioclase and K-feldspar, which is consistent with the negative correlation between log E and log Ba (Fig. 14e). The TSHT granites have low total concentrations of REE (less than 120 ppm), which could be attributed to fractional crystallization of REE-enriched accessory mineral, such as apatite and monazite. The La vs. (La/Yb)_N diagram (Fig. 14f) reveals that the REE chondrite-normalized diagram in the TSHT granites are likely controlled by crystallization of monazite and/or allanite.

The TSHT granites occur contemporaneously and spatially related to the TSHT mafic rock, suggesting the former could be formed by the enrichment of fractional crystallization of monazite and/or allanite.

5.2. Petrogenesis of the TSHT granites

The TSHT granites have relatively high concentrations of SiO₂ (75.14–79.57%) and high negative E anomalies ($E/E^* = 0.02-0.09$) and are depleted in Ba, Sr, P in the primitive-mantle-normalized diagram (Fig. 7f). They exhibit low ratios of 1000*Ga/Al (2.23–2.65) and (Na₂O + K₂O)/CaO (5.15–9.45), and low concentrations of Zr (96.6–146 ppm) and Zr + Nb + Ce + Y (207–345 ppm), both lower than the lower limits of the typical A-type granites (Collin et al., 1982; Whalen et al., 1987). Most TSHT granites plot in the fractionated granite field on the diagram of Zr + Nb + Ce + Y vs. (Na₂O + K₂O)/CaO (Fig. 14a). The characteristic of the TSHT granites reveals that they are high-*K* fractionated granites, as indicated by their low concentrations of Fe₂O₃ and MgO. Unfractionated granites all have a relationship with a ratio of Zr/Hf in HFSE elements, such as Zr/Hf and Nb/Ta (Green, 1995). While the ratio will decrease obviously when the magma type is changing in the fractionation (e.g., Pêre-Soba and Villaeca, 2010). The TSHT granites have low ratios of Zr/Hf (22.5–28.9) and Nb/Ta (4.25–7.90) relative to typical granites (38 for Zr/Hf and 17 for Nb/Ta), which is consistent with the mafic differentiation.

The TSHT granites have relatively low concentrations of Al₂O₃ (11.80–13.85%) and are alkali-felsic (most lower than 1.10), which is distinct from typical S-type granites (Chappell, 1999).

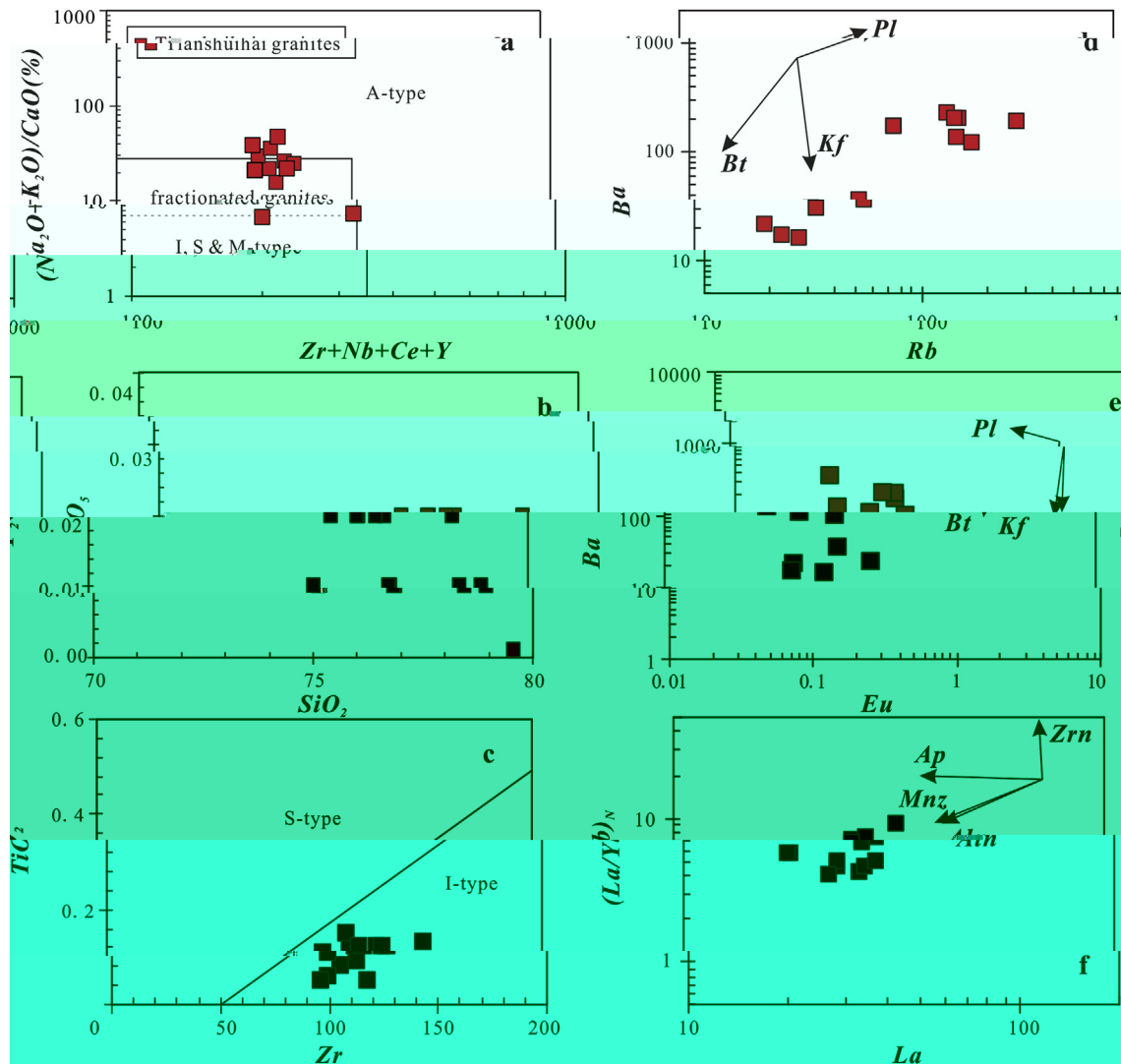


Fig. 14. (a) Zr + Nb + Ce + Y vs. $(\text{Na}_2\text{O} + \text{K}_2\text{O})/\text{CaO}$, (b) SiO_2 vs. P_2O_5 and (c) Zr vs. TiO_2 diagram showing fractionated I-type granite signature for the granitic rock from Tianshūihai terrane. (d) Rb vs. Ba and (e) Eu vs. Ba diagram showing crystallization of plagioclase and (f) $(\text{La}/\text{Yb})_N$ vs. La vs. $(\text{La}/\text{Yb})_N$ diagram showing crystallization of monomineral and/or allanite.

The final closure of the Moambiqe Ocean between East Gondwana and West Gondwana at ca. 540–530 Ma formed the Great Gondwana (Fig. 15a, Collin and Piarek, 2005; Li et al., 2008), as evidenced by the palaeomagnetic data (Meer and Van der Voo, 1996), causing the final docking of India to Australia-East Antarctica along the Pinjarra Orogen (Boger and Miller, 2004; Collin and Piarek, 2005). Episodic bioproxy connections in the East Gondwana during the Early- to mid-Paleozoic indicated the micro-continent distributed in East Antarctica, including the Tarim, Qaidam, Qilian, South China Block (SCB), North China Block (NCB), Alek, Sibma and Indochina, were located near Australia (Fig. 15b, Meccalfe, 2011, 2013).

The Archean MZT and the Neoproterozoic TSHT are two identified Precambrian basements in the WKOB (Zhang et al., 2018c, d). Although the MZT and the TSHT are different in age, they are all confirmed Precambrian basements in the WKOB. Considering the similarities of the Early Paleozoic accretionary complex of BKG and Sai la Group (Zhang et al., 2018a, c), distributed to the north of the MZT and TSHT, respectively, it is possible that the MZT and TSHT are a whole before the early Cambrian (ca. 530 Ma). This conclusion is further supported by the

paleogeographic evidence of the northern margin of the Tarim Block (Huang et al., 2011). According to the paleogeographic reconstruction of Li et al. (2018), the place of the MZT-TSHT between the Tarim and East Gondwana (Fig. 15b). The MZT probably is the Archean (ca. 2.5 Ga) bimodal meta-igneous rock overprinted by ca. 2.0 Ga metamorphism and Neoproterozoic (ca. 840 Ma) granitic magmatism (Zhang et al., 2018b), which have morphological similarities to the Archean Kongling complex in the SCB (Zhang and Zheng, 2013). Further, the detritalircon of the felsic gabbroedimentar sequence in the TSHT shared similar age spectra to the late Neoproterozoic sequence from SCB (Huang et al., 2016; Zhang et al., 2015, 2018c). Precambrian rock assemblage, phases of igneous activities and metamorphism of the MZT-TSHT have morphological similarities to the SCB, which argued that the terrane is a continental fragment detached from SCB during the breakup of the Rodinia Supercontinent. The BKG as an early Cambrian (530–508 Ma, Zhang et al., 2018a) accretionary wedge between the Tarim and the MZT. The Early Cambrian (ca. 530 Ma) gabbro sheet and ophiolite emplaced in the lower part of the BKG were regarded to be derived from a metamorphosed ophiolite sequence in a fore-arc setting (Zhang et al., 2018d). The ca. 530 Ma arc-like dolerite/

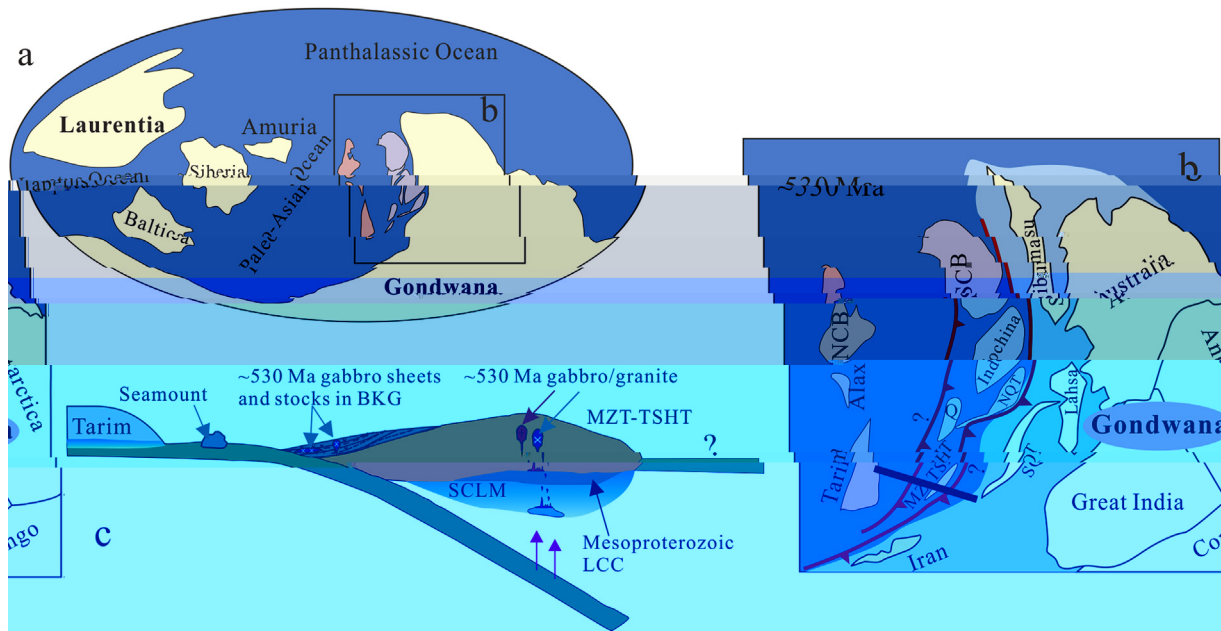


Fig. 15. Early Cambrian (~530 Ma) global continental/micro-continental block distribution (a) and possible distribution of the block at the northern fringe of Gondwana (b, Modified from Li et al., 2018; McCalfe et al., 2011, 2013). (c) Cartoon model showing the formation of Cambrian dolerite-gabbro in the MZT-TSHT and the initiation of Pro-O-Tethyan oceanic subduction at ca. 530 Ma (the thickness of the SCLM and crustal thickness are not scaled). BKG—Cambrian Block; Q—Qaidam; SCB—South China Block; NCB—North China Block; SQT—South Qiangang; NQT—North Qiangang; MZT-TSHT—Maar Terrane-Tianhai Terrane. See details in the text.

gabbro intrusion in the TSHT or the BKG a coeval dolerite-gabbro sheet and ock emplaced in the lower part of the BKG (Zhang et al., 2018d), which formed the initial magmatic arc of the orogenic belt of the Pro-O-Tethyan Ocean (Fig. 15c). The continental orogenic belt of the Pro-O-Tethyan Ocean led to the metamorphism of the SCLM beneath the MZT. Partial melting of the mafic intrusion enriched mantle source (SCLM) generated the mafic intrusion in the MZT.

Volcanic early Paleozoic granite emplaced in the SKT and the TSKT during 510–400 Ma (Jiang et al., 2002, 2008; Zhang et al., 2018a, 2018b). The granite has variable geochemical composition, including the 430 Ma adakitic rock (Ye et al., 2008; Wang et al., 2017), which may be related from partial melting of the thickened lower crust (Wang et al., 2017). The thickening of the continental crust in an orogenic belt can be acribed to the continental-continental collision, such as the Dabie Orogenic Belt and Tibe Plateau (Cheng et al., 2003; Wang et al., 2007), indicating the final collision between the Tarim Block and East Gondwana earlier than 430 Ma. Overall, coupled with the occurrence of ca. 440 Ma amphibolite-facies metamorphism of the SKT, documents the accretion between Tarim and TSHT finalized at ca. 440 Ma (Zhang et al., 2018c). The closure of the Pro-O-Tethyan Ocean led to the final amalgamation of the block in the Northern Tibe and Asia, including the Tarim, MZT-TSHT, Qaidam, SCB, Indochina, etc., on the northern margin of the East Gondwana (McCalfe, 2011, 2013).

6. Conclusions

- (1) The granitic intrusion in Tianhai Terrane were emplaced at ca. 530 Ma, coeval with the dolerite-gabbro in this area and the gabbro sheet and ock emplaced in the lower part of the Cambrian accretionary wedge. The dolerite-gabbro from the Maar Terrane was emplaced at ca. 500–490 Ma.
- (2) The dolerite/gabbroic intrusion in Tianhai Terrane were derived from a depleted mantle source in an initial

subduction zone; hereafter the mafic intrusion in Maar Terrane were generated from a sub-continental lithospheric mantle source in an arc setting.

- (3) A Cambrian magmatic arc, genetically related to the orogenic belt of the Pro-O-Tethyan Ocean during 530–490 Ma, developed along the Maar-Tianhai Terrane. The final closure of the Pro-O-Tethyan Ocean occurred at ca. 440 Ma, which led to the errance along the northern margin of the Tibe Plateau and East Asia docked onto the East Gondwana.

Acknowledgements

We sincerely thank Mr. Wen-Hai Ji for his help in the field work and providing the 1/50000 geological map. We are grateful to Dr. Wei Xie for his assistance in SHRIMP zircon dating and to Dr. Jian Zhang for LA-MC-ICPMS zircon dating and in situ U–Hf isotope analysis. This project is funded by the National 305 Project of China (2018A03004-1, 2015BAB05B01-1) and the Fundamental Research Funds for the Central Universities (2019B18914).

Appendix A. Supplementary data

Supplementary data to this article can be found online at <http://doi.org/10.1016/j.litho.2019.105226>.

References

- Boger, S.D., Miller, J.M., 2004. Terminal rifting of Gondwana and the onset of the Rodinia–Delamerian orogen: the cause and effect of an Early Cambrian reconfiguration of plate motion. *Earth Planet. Sci. Lett.* 219, 35–48.
- Chappell, B.W., 1999. Aluminium saturation in I- and S-type granites and the characteristic of fractionated haplogranites. *Lithos* 46, 535–551.
- Cheng, S.L., Li, D.Y., Ji, J.Q., Chen, M.F., Lee, H.Y., Wen, D.J., Luo, C.H., Lee, T.Y., Qian, Q., Zhang, Q., 2003. Adakite from continental collision zone: melting of thickened lower crust beneath the northern Tibe Plateau. *Geology* 31, 1021–1024.
- Collin, W.J., Beam, S.D., Whie, A.J.R., Chappell, B.W., 1982. Nature and origin of A-type granites: a hypothetical reference to the eastern Australia. *Contrib. Mineral. Petrol.* 80 (2), 189–200.
- Collin, A.S., Piarek, S.A., 2005. Amalgamation of eastern Gondwana: the collision

- of the Circum-Indian orogen. *Earth Sci. Res.* 71, 229–270.
- Ci, J.T., Bian, X.W., Wang, G.B., 2006. Geological composition and evolution of the Kailashan. *Geol. Shaanxi* 24, 1–11 (in Chinese with English abstract).
- Ducea, M.N., Hoesly, M.A., Kidder, S., 2003. Bifurcating the Pamir: the evolution of the Indian Plate. *Geology* 31, 849–852.
- Geng, J.Z., Li, H.K., Zhang, J., Zhang, Y.Q., 2011. Zircon Hf isotope analysis of LA-MC-ICP-MS. *Geol. Bull. China* 30, 1508–1513 (in Chinese with English abstract).
- Green, T.H., 1995. Significance of Nb/Ta as an indicator of geochemical processes in the crust. *Earth Planet. Chem. Geol.* 120, 347–359.
- Gibson, A.D., Zhi, R.C., Searles, R.D., Whittaker, J.M., Yeh, H., 2015. A tectonic model reconciling the evidence for the collision between India, Eurasia and the intra-oceanic arc of the central-eastern Tethys. *Gondwana Res.* 28, 451–492.
- Han, Y.G., Zhao, G.C., Cao, P.A., Sun, M., Eissner, P.R., Ho, W.Z., Zhang, X.R., Li, Q., 2016. Tarim and North China cratons linked to the northern Gondwana through the collisional orogenic and collisional orogenic belts. *Geology* 44, 95–98.
- Harker, A.B., Gallagher, K., Herg, J.M., McDermott, F., 1993. Mantle and slab contributions to arc magmas. *Ann. Rev. Earth Planet. Sci.* 21, 175–204.
- Harker, A.B., Herg, J.M., Tegner, S.P., McDermott, F., Peacock, D.W., Van Calsteren, P., 1997. U–Th isotope in arc magma: implications for element transfer from the mantle to the crust. *Science* 276, 551–555.
- Hofmann, A.W., 1988. Chemical differentiation of the Earth: the relationship between mantle, continental crust, and oceanic crust. *Earth Planet. Sci. Lett.* 90, 297–314.
- Hofmann, A.W., 2003. Sampling mantle heterogeneities through oceanic basalts: isotope and trace element geochemistry. *Earth Planet. Chem. Geol.* 2, 61–101.
- Hou, J., Wang, H., Huang, C.Y., Tong, L.X., Miao, S.L., Qi, Z.W., 2016. Geological characteristics and age of the Dahongliang Fe-ore deposit in the Weibei orogenic belt, Xinjiang, north of the eastern China. *J. Asian Earth Sci.* 116, 1–25.
- Huang, X.L., Ni, Y.L., Xu, Y.G., Chen, L.L., Yang, Q.J., 2010. Mineralogical and geochemical constraints on the petrogenesis of post-collisional and-orogenic magmas from the eastern Yunnan, SW China. *J. Petrol.* 51, 1617–1654.
- Huang, H.F., Wang, J., Gao, L.Z., 2011. Oceanic and continental framework of Early Cambrian period in Tarim area. *Chin. Geol.* 38, 980–988 (in Chinese with English abstract).
- Ji, W.H., Li, R.S., Chen, S.J., He, S.P., Zhao, Z.M., Bian, X.W., Zhang, H.P., Cui, J.G., Ren, J.G., 2011. The diagenetic evolution of volcanic rocks in the Beilunkou Group from the Tianhuai area in Xinjiang of north of the eastern China and its geological significance. *Sci. China (D-Earth Planet. Sci.)* 54, 61–72.
- Jiang, C.F., Yang, J.S., Feng, B.G., Zhang, Z.Z., Zhao, M., Chai, Y.C., Shi, X.D., Wang, H.D., Han, J.Q., 1992. Opening-closure of the Kailashan tectonic zone. In: *Geol. Memoir*, vol. 5. Geological Publishing House, Beijing, p. 224 (in Chinese with English abstract).
- Jiang, Y.H., Jiang, S.Y., Ling, H.F., Zhou, X.R., Ren, J.X., Yang, W.Z., 2002. Petrology and geochemistry of high-alumina plagioclase from the eastern Kailashan orogenic belt, north of the eastern Xinjiang, China: implications for granulite facies. *Lithos* 63, 165–187.
- Jiang, Y.H., Liao, S.Y., Yang, W.Z., Shen, W.Z., 2008. An island arc origin of plagioclase and orthopyroxene in the eastern Kailashan orogen, North of the eastern China: SHRIMP U–Pb chronology, elemental and Sr–Nd–Hf isotope geochemistry and Paleozoic tectonic implications. *Lithos* 106, 323–335.
- Jiang, Y.H., Jia, R.Y., Li, Z., Liao, S.Y., Zhao, P., Zhou, Q., 2013. Origin of Middle Triassic high-K calc-alkaline granulite and their post-orogenic microgranular enclaves from the Weibei orogen, north of the eastern China: a record of the closure of Paleotethys. *Lithos* 156–159, 13–30.
- Leake, B.E., Wooley, A.R., Arps, C.E.S., Birch, W.D., Gilber, M.C., Grice, J.E., Hawthorne, F.C., Kato, A., Kishida, H.J., Krieger, V.G., Lin, H., K., Laird, J., Mandarino, J.A., Marek, V.V., Nickel, E.H., Rock, N.M.S., Schumacher, J.C., Smit, D.C., Sphenon, N.C.N., Ungaretti, L., Whittaker, E.J.W., Yoder, H.G., 1997. Nomenclature of amphibole: report of the Subcommittee on amphibole of the International Mineralogical Association, Commission on mineral names. *Can. Mineral.* 35, 219–246.
- Li, S.Z., Zhao, S.J., Li, X., Cao, H., Yu, S., Li, X.Y., Somerville, I., Yu, S.Y., 2018. Closure of the Pro-Tethys ocean and early Paleozoic amalgamation of microcontinents in the East Asia. *Earth Sci. Res.* 186, 37–75.
- Li, X.H., Li, Z.X., Wingate, M.T.D., Cheng, S.L., Li, Y., Lin, G.C., Li, W.X., 2006. Geochemistry of the 755 Ma Mandine Well dyke swarm, north of the East Asia: part of a Neoproterozoic mantle plume beneath Rodinia? *Precambrian Res.* 146, 1–15.
- Li, X.H., Li, W.X., Li, Z.X., 2007. On the genetic classification and tectonic implications of the early Yunnanian granulites in the Nanling range, South China. *Chin. Sci. Bull.* 52 (14), 1873–1885.
- Li, Z.X., Bogdanov, S.V., Collins, A.S., Davidson, A., DeWaele, B., Ernst, R.E., Fiala, I.C.W., Fiala, R.A., Gladkoch, D.P., Jacob, J., Karlstrom, K.E., Li, S., Naipao, L.M., Pea, V., Piarck, S.A., Thrane, K., Vernikoff, V., 2008. A tectonic configuration, and break through of Rodinia: a synthesis. *Precambrian Res.* 160, 179–210.
- Liao, S.Y., Jiang, Y.H., Jiang, S.Y., Yang, W.Z., Jin, G.D., Zhao, P., 2010. Sbd cing ediment-derived arc granulites: Evidence from the Dandong pluton and its quartz-enriched enclaves in the eastern Kailashan orogen, north of the eastern China. *Mineral. Petrol.* 100, 55–74.
- Li, Z., Jiang, Y., Jia, R., Zhao, P., Zhou, Q., 2015. Origin of Late Triassic high-K calc-alkaline granulite and their post-orogenic microgranular enclaves from the eastern Tethys Plateau, north of the eastern China: implications for Paleotethyan evolution. *Gondwana Res.* 27, 326–341.
- Lidz, K.R., 2003. *U–Th–Pb Manual for Isotope 3.00: A Geochronological Toolkit for Microanalysis*. Elsevier, Amsterdam.
- Ma, P., Tappinier, P., Arnaud, N., Borjesson, L., Aouac, J.P., Vidal, Ph., Li, Q., Pan, Y.S., Wang, Y., 1996. Tectonic evolution of the eastern Tethys, between the Tarim and the Indian Plate. *Sci. Lett.* 142, 311–330.
- Ma, F., Schneider, W., 2000. Setting of the Pro- and paleo-Tethyan Ocean in the eastern Kailashan (Xinjiang, China). *J. Asian Earth Sci.* 18, 637–650.
- McClough, M.T., Gregor, R.T., Warburg, G.J., Taylor, H.P., 1981. Sm–Nd, Rb–Sr, and 180/160 oxygen isotope geochemistry in an oceanic crustal section: evidence from the Samail ophiolite. *J. Geophys. Res.* 86, 2721–2735.
- Meer, J.G., Van der Voo, R., 1996. Paleomagnetic and 40Ar/39Ar dating of the Indian dolerite Ken a: implications for Gondwana tectonics. *J. Geol.* 104, 131–142.
- McClough, M.T., 2011. Paleozoic tectonics of the SE Asia. In: Hall, R., Coombs, M., Wilton, M. (Eds.), *The Southeast Asian Geology: History and Tectonics of a Tethyan–Gondwanan Collision*, vol. 355. Geological Society of London Special Publication, pp. 7–35.
- McClough, M.T., 2013. Gondwanan dispersion and Asian accretion: tectonic and palaeogeographic evolution of the eastern Tethys. *J. Asian Earth Sci.* 66, 1–13.
- Molina, J.F., Scarro, J.H., Monero, P.G., Bea, F., 2009. High-Ti amphibole as a petrogenetic indicator of magma chemistry: evidence for mildly alkaline high-temperature melting of the Variscan Iberian orogenic belt. *Contrib. Mineral. Petrol.* 158, 69–98.
- Pan, Y.S., 1990. Tectonic evolution and evolution of the eastern Kailashan tectonic zone. *Earth Sci. Res.* 3, 224–232 (in Chinese with English abstract).
- Pan, Y.S., 1996. Geological evolution of the Karakoram and Kailashan tectonic zones. *Seismological Press, Beijing*, pp. 34–78.
- Pan, Y.S., Wang, Y., 1994. Diagenetic evolution and evidence of the fifth tectonic zone of the Qinghai–Tibet Plateau. *Acta Geophys. Sin.* 37, 241–250 (in Chinese with English abstract).
- Pearce, J.A., Thirlall, M.F., Ingram, G., Morrison, B.J., Arculus, R.J., Van der Laan, S.R., 1992. Isotopic evidence for the origin of boninites and related rocks drilled in the I-Bonin (Ogasawara) forearc, Leg 125. In: *Proceedings of the Ocean Drilling Program*, vol. 125. Scientific Results, pp. 237–261.
- Pérez-Soba, C., Villaeca, C., 2010. Petrogenesis of high-temperature peraluminous granites in the Iberian Peninsula (Spanish Central System). *Geol. Acta* 8, 131–149.
- Ringwood, A.E., 1974. *The Petrological Evolution of the Island Arc System*. [J], vol. 130. Journal of Geological Society, London, 183–20.
- Robin, A.C., Yin, A., Manning, C.E., Harri, T.M., Zhang, S.-H., Wang, X.-F., 2007. Cenozoic evolution of the eastern Pamir: implications for rain accommodation mechanisms at the eastern end of the Himalayan–Tibetan Orogen. *GSA Bulletin* 119, 882–896.
- Robin, A.C., Ducea, M., Lapen, T.J., 2012. Deformation and isotope constraints on the crustal architecture and tectonic evolution of the northern Pamir. *Tectonics* 31, 1–16.
- Rudnick, R.L., Gao, S., 2003. Composition of the continental crust. In: Rudnick, R.L. (Ed.), *The Crust: Treatise on Geochemistry*, vol. 3. Elsevier-Perгамon, Oxford, UK, pp. 1–64.
- Rudnick, R.L., Raebacher, L., Schneider, S., Sberner, K., Searns, M.A., Gilmer, M.A., Hacker, B.R., 2017. Bifurcating the Pamir–Tibet Plateau–crustal thickening, extensional collapse, and lateral erosion in the Central Pamir: 1. Geometry and kinematics. *Tectonics* 36 (3), 342–384.
- Schub, M., Raebacher, L., Siebel, W., Williams, M.M., Minaev, V., Lokko, V., Chen, F., Saneck, K., Nelson, B., Friedrich, W., Wooden, J.L., 2004. A tectonic evolution of the Pamir: age and origin of magma bodies from the northern Tianshan or the northern Pamir and their relationship to the Tethys. *Tectonics* 23, 1–31.
- Seely, E., 1893. Are great ocean depths permanent? *Nature* 52, 180–187.
- Sun, S.S., McDonough, W.F., 1989. Chemical and isotopic geochemistry of oceanic basalts: implications for mantle composition and processes. In: *Sunder, A.D., Morr, M.J.* (Eds.), *Magma in the Ocean Basin*, vol. 42. Geological Society of London Special Publication, pp. 528–548.
- Wang, Q., Wang, D.A., Xu, J.F., Jian, P., Zhao, Z.H., Li, C.F., Xu, W., Ma, J.L., He, B., 2007. Early Cretaceous adakitic granites in the North Dabie Complex, Central China: implications for partial melting and delamination of the thickened lower crust. *Geochimica et Cosmochimica Acta* 71, 2609–2636.
- Verhoogen, J.D., Paiche, P.J., Blicher-Tof, J., Albareda, F., 1999. Relationship between the Hf–Nd and Sm–Nd isotope geochemistry in the global orogenic belts. *Earth Planet. Sci. Lett.* 168, 79–99.
- Wang, Z.H., 2004. Tectonic evolution of the Weibei orogenic belt, eastern China. *J. Asian Earth Sci.* 24, 153–161.
- Wang, Z.H., Sun, S., Ho, Q.L., Li, J.L., 2001. Effect of melt-rock interaction on geochemistry in the Kailashan ophiolite (Weibei orogenic belt, north of the eastern China): implications for ophiolite origin. *Earth Planet. Sci. Lett.* 191, 33–48.
- Wang, Z.H., Sun, S., Li, J.L., Ho, Q.L., 2002. Petrogenesis of the ophiolite and its relationship to the Kailashan orogenic belt (Weibei orogenic belt, north of the eastern China): implications for the evolution of back-arc basins. *Contrib. Mineral. Petrol.* 143, 471–483.
- Wang, J., Harri, K., Li, J.G., Song, Y., Gao, Y.B., Zhang, H., 2017. Shoshonitic and adakitic magmas in the Early Paleozoic age in the Weibei orogenic belt, NW China: implications for the early evolution of the northern Tethys Plateau. *Lithos* 286–287, 345–362.
- Whalen, J.B., Currie, K.L., Chappell, B.W., 1987. Aluminous granites: geochemical characteristics, diagenesis and petrogenesis. *Contrib. Mineral. Petrol.* 95 (4), 407–419.
- Williams, I.S., 1998. U–Th–Pb geochronology by microprobe. *Rev. Econ. Geol.* 7, 1–35.

- Wolf, M.B., London, D., 1994. Age and diagenesis of ophiolite in ophiolite melange: an example from the ophiolite and mechanical. *Geochem. Cosmochim. Acta* 58 (19), 4127–4254.
- Wu, F.Y., Jahn, B.M., Wilder, S.A., 2003. Highlithification of I-type granites in NE China (I): geochronology and petrogenesis. *Lithos* 66 (3/4), 241–273.
- Xiao, W.J., Ho, Q.L., Li, J.L., Windle, B.F., Hao, J., Fang, A.M., Zhou, H., Wang, Z.H., Chen, H.L., Zhang, G.C., Yan, C., 2000. Tectonic face and the archipelago-accretion process of the Weikang, China. *Sci. China (Series D)* 43, 134–143.
- Xiao, W.J., Li, J.L., Ho, Q.L., Zhang, G.C., Chen, H.L., 1998. Structural evolution of the Sohearn Weikang and its implication for growing orogenesis. *Acta Geologica Sinica* 41, 133–141.
- Xiao, W.J., Windle, B.F., Hao, J., Li, J.L., 2002a. Arc-ophiolite obduction in the eastern Kangle range (China): implication for the palaeozoic evolution of central Asia. *J. Geol. Soc.* 159, 517–528.
- Xiao, W.J., Windle, B.F., Chen, H.L., Zhang, G.C., Li, J.L., 2002b. Carboniferous–Triassic obduction and accretion tectonics of the northern Tibetan Plateau. *Geology* 30, 295–298.
- Xiao, W.J., Windle, B.F., Li, D.Y., Jian, P., Li, C.Z., Yan, C., Sun, M., 2005. Accretionary tectonics of the eastern Kangle orogen, China: a Paleozoic–Early Mesozoic, long-lived active continental margin with implication for the growth of northern Eurasia. *J. Geol.* 113, 687–705.
- Yang, J.S., Robinson, P.T., Jiang, C.F., Xu, Z.Q., 1996. Ophiolite of the Kangle Moinean, China and their tectonic implication. *Tectonophysics* 258, 215–231.
- Ye, H.M., Li, X.H., Li, Z.X., Zhang, C.L., 2008. Age and origin of the high Ba–Sr granitoid from northern Qinghai–Tibet Plateau: implication for the early Paleozoic tectonic evolution of the Weikang orogenic belt. *Gondwana Research* 13, 126–138.
- Yin, A., Harrison, T.M., 2000. Geologic evolution of the Himalayan–Tibetan orogen. *Ann. Rev. Earth Planet. Sci.* 28, 211–280.
- Yan, C., Sun, M., Zhou, M.F., Zhou, H., Xiao, W.J., Li, J.L., 2002. Tectonic evolution of the Weikang: geochronological and geochemical constraints from Kangle granitoid. *Int. J. Geol. Res.* 44, 653–669.
- Yan, C., Sun, M., Yang, J.S., Zhou, H., Zhou, M.F., 2004. In: Nb-depleted, Conical at Rif–Relaxed Alkali Mafic Volcanic Rock (Weikang): Implication for the Rifting of the Tarim Craton from Gondwana. *Geological Society, London, Special Publication*, pp. 131–143.
- Yan, C., Sun, M., Zhou, M.F., Xiao, W.J., Zhou, H., 2005. Geochemistry and petrogenesis of the Yihak volcanic sequence, Kangle ophiolite, Weikang (NW China): implication for the magmatic evolution in a subduction zone environment. *Contrib. Mineral. Petrology* 150, 195–211.
- Zhang, C.L., Yu, H.F., Shen, J.L., Dong, J.G., Ye, H.M., Guo, K.Y., 2004. Zircon SHRIMP age determination of the gabbro and basalts in the Kangle ophiolite: membership of the Kangle ophiolite. *Geol. Res.* 50, 639–643 (in Chinese with English abstract).
- Zhang, C.L., Yu, H.F., Ye, H.M., Wang, A.G., 2006. Age, geochemistry, petrogenesis and tectonic implication. *Science in China (Series D)* 49, 1121–1134.
- Zhang, C.L., Li, S.N., Yu, H.F., Ye, H.M., 2007. Tectonic evolution of the Weikang Orogenic belt: evidence from zircon SHRIMP and LA-ICP-MS U–Pb age. *Science in China (Series D)* 50, 1–12.
- Zhang, C.L., Ye, X.T., Zou, H.B., Chen, X.Y., 2016. Neoproterozoic edimentation and evolution in the eastern Tarim, NW China: new evidence from field observations, detrital zircon U–Pb age and Hf isotope composition. *Precambrian Res.* 280, 31–45.
- Zhang, C.L., Zou, H.B., Ye, X.T., Chen, X.Y., 2018a. Tectonic evolution of the NE extension of the Pamir Plateau: new evidence from field observations and zircon U–Pb geochronology. *Tectonophysics* 723, 27–40.
- Zhang, C.L., Zou, H.B., Ye, X.T., Chen, X.Y., 2018b. A newly identified Precambrian errane in NE Pamir: the Archean basement and Neoproterozoic granitic intrusion. *Precambrian Res.* 304, 73–87.
- Zhang, C.L., Zou, H.B., Ye, X.T., Chen, X.Y., 2018c. Tectonic evolution of the eastern extension of the Weikang Orogenic Belt at the northern margin of the Tibetan Plateau: new evidence from field observations and geochronology. *Geochimica et Cosmochimica Acta* <https://doi.org/10.1016/j.gca.2018.05.006>.
- Zhang, C.L., Zou, H.B., Ye, X.T., Chen, X.Y., 2018d. Timing of obduction initiation in the Pro-Tethyan ocean: evidence from the Cambrian gabbro from the NE Pamir Plateau. *Lithos* 314 (315), 40–51.
- Zhang, S.B., Zheng, Y.F., 2013. Formation and evolution of Precambrian continental lithosphere in South China. *Gondwana Research* 23, 1241–1260.
- Zhang, S.B., He, Q., Zheng, Y.F., 2015. Geochronological and geochemical evidence for the nature of the Dongling complex in South China. *Precambrian Res.* 256, 17–30.
- Zhao, G.C., Wang, Y.J., Huang, B.C., Dong, Y.P., Li, S.Z., Zhang, G.W., Yu, S., 2018. Geological Reconstruction of the East Asian Block: from the Breakup of Rodinia to the Assembly of Pangea. *Earth-Science Reviews*. In Press.
- Zhou, J., Li, Q.G., Chen, X., Tang, H.S., Wang, Z.Q., Chen, Y.J., Li, S.W., Xiao, B., Chen, J.L., 2017. Geochemistry and petrogenesis of the early Palaeozoic appinitic granites complex in the Weikang Orogenic Belt, NW China: implication for Palaeozoic tectonic evolution. *Geol. Mag.* <https://doi.org/10.1017/S0016756817000450>.